FIRST LIGHT LBT AO IMAGES OF HR 8799 bcde AT 1.6 AND 3.3 μm: NEW DISCREPANCIES BETWEEN YOUNG PLANETS AND OLD BROWN DWARFS[*]

ANDREW J. SKEMER[1], PHILIP M. HINZ[1], SIMONE ESPOSITO[2], ADAM BURROWS[3], JARRON LEISENRING[4], MICHAEL SKRUTSKIE[5], SILVANO DESIDERA[6], DINO MESA[6], CARMELO ARCIDIACONO[2,7], FILIPPO MANNUCCI[2], TIMOTHY J. RODIGAS[1], LAIRD CLOSE[1], DON MCCARTHY[1], CRAIG KULESA[1], GUIDO AGAPITO[2], DANIEL APAI[1,8], JAVIER ARGOMEDO[2], VANESSA BAILEY[1], KONSTANTINA BOUTSIA[9,10], RUNA BRIGUGLIO[2], GUIDO BRUSA[9], LORENZO BUSONI[2], RICCARDO CLAUDI[6], JOSHUA EISNER[1], LUCA FINI[2], KATHERINE B. FOLLETTE[1], PETER GARNAVICH[11], RAFFAELE GRATTON[6], JUAN CARLOS GUERRA[9], JOHN M. HILL[9], WILLIAM F. HOFFMANN[1], TERRY JONES[12], MEGAN KREJNY[12], JARED MALES[1], ELENA MASCIADRI[2], MICHAEL R. MEYER[4], DOUGLAS L. MILLER[9], KATIE MORZINSKI[1], MATTHEW NELSON[5], ENRICO PINNA[2], ALFIO PUGLISI[2], SASCHA P. QUANZ[4], FERNANDO QUIROS-PACHECO[2], ARMANDO RICCARDI[2], PAOLO STEFANINI[2], VIDHYA VAITHEESWARAN[1], JOHN C. WILSON[5], AND MARCO XOMPERO[2]

[1] Steward Observatory, Department of Astronomy, University of Arizona, 933 N. Cherry Ave, Tucson, AZ 85721, USA
[2] Istituto Nazionale di Astrofisica, Osservatorio Astrofisico di Arcetri, Largo E Fermi 5, 50125 Firenze, Italy
[3] Department of Astronomy, Princeton University, 4 Ivy Lane, Princeton, NJ 08544, USA
[4] Institute for Astronomy, ETH Zurich, Wolfgang-Pauli-Strasse 27, CH-8093 Zurich, Switzerland
[5] Department of Astronomy, University of Virginia, 530 McCormick Road, Charlottesville, VA 22904, USA
[6] Istituto Nazionale di Astrofisica, Osservatorio Astronomico di Padova, Vicolo dell' Osservatorio 5, I-35122 Padova, Italy
[7] Istituto Nazionale di Astrofisica, Osservatorio Astronomico di Bologna, Via Ranzani 1, 40127 Bologna, Italy
[8] Department of Planetary Sciences, University of Arizona, 1629 E. University Blvd., Tucson, AZ 85721, USA
[9] Large Binocular Telescope Observatory, University of Arizona, 933 N. Cherry Ave, Tucson, AZ 85721, USA
[10] Istituto Nazionale di Astrofisica, Osservatorio Astronomico di Roma, Via Frascati 33, 00040 Rome, Italy
[11] Department of Physics, University of Notre Dame, 225 Nieuwland Science Hall, Notre Dame, IN 46556, USA
[12] School of Physics and Astronomy, University of Minnesota, 116 Church Street S.E., Minneapolis, MN 55455, USA

ABSTRACT

As the only directly imaged multiple planet system, HR 8799 provides a unique opportunity to study the physical properties of several planets in parallel. In this paper, we image all four of the HR 8799 planets at H band and 3.3 μm with the new Large Binocular Telescope adaptive optics system, PISCES, and LBTI/LMIRCam. Our images offer an unprecedented view of the system, allowing us to obtain H and 3.3 μm photometry of the innermost planet (for the first time) and put strong upper limits on the presence of a hypothetical fifth companion. We find that all four planets are unexpectedly bright at 3.3 μm compared to the equilibrium chemistry models used for field brown dwarfs, which predict that planets should be faint at 3.3 μm due to CH_4 opacity. We attempt to model the planets with thick-cloudy, non-equilibrium chemistry atmospheres but find that removing CH_4 to fit the 3.3 μm photometry increases the predicted L' (3.8 μm) flux enough that it is inconsistent with observations. In an effort to fit the spectral energy distribution of the HR 8799 planets, we construct mixtures of cloudy atmospheres, which are intended to represent planets covered by clouds of varying opacity. In this scenario, regions with low opacity look hot and bright, while regions with high opacity look faint, similar to the patchy cloud structures on Jupiter and L/T transition brown dwarfs. Our mixed-cloud models reproduce all of the available data, but self-consistent models are still necessary to demonstrate their viability.

Key words: brown dwarfs – instrumentation: adaptive optics – planetary systems – planets and satellites: atmospheres – stars: individual (HR 8799)

Online-only material: color figures

1. INTRODUCTION

Efforts are underway to characterize the first generation of directly imaged extrasolar planets. A principal focus has been the HR 8799 planetary system (Marois et al. 2008, 2010), which with four planets is currently unique as a directly imaged multiple-planet system. Studying these planets simultane-

ously is particularly powerful given their connected formation histories and appearances.

HR 8799 is a young, A5V star with a λ Boo deficiency of heavy metals and three distinct circumstellar dust structures (Marois et al. 2008; Cowley et al. 1969; Gray & Kaye 1999; Su et al. 2009). There is some disagreement about the age of the system. Traditional age-dating methods, such as galactic space motion and Hertzsprung–Russell diagram position, suggest that HR 8799 has an age of 20–160 Myr (Moór et al. 2006; Marois et al. 2008; Hinz et al. 2010; Zuckerman et al. 2011), while astroseismology estimates are more consistent with ~1 Gyr, which would make the planets significantly more massive brown dwarfs (Moya et al. 2010). Interestingly, the dynamical stability of the planets themselves places upper limits on the masses of the planets (Fabrycky & Murray-Clay 2010; Moro-Martín et al.

2010; Sudol & Haghighipour 2012), which directly converts to a young system age, based on the planets' photometry and evolutionary models (Burrows et al. 1997; Chabrier et al. 2000).

An important implication of the relative youth and low masses of the HR 8799 planets is that their appearances and atmospheric properties might be different than field brown dwarfs, which can have the same effective temperatures as giant planets while being older and more massive. Brown dwarf spectra have been used as proxies for giant planet spectra to plan direct imaging surveys and to interpret early discoveries. However, initial results show that there are several key differences between the atmospheres of giant exoplanets and brown dwarfs.

For field brown dwarfs, the L→T spectral-type transition occurs at ∼1200–1400 K, where dust clouds settle/condense below the photosphere (Saumon & Marley 2008), and CO is converted to CH_4 (Burrows et al. 2003; Geballe et al. 2002). For the HR 8799 planets, clouds are suspended in the photosphere at lower effective temperatures (900–1200 K) than is typical for brown dwarfs (Currie et al. 2011; Madhusudhan et al. 2011; Barman et al. 2011a). Additionally, there appears to be more CO than CH_4 relative to equilibrium chemistry models, implying that convection is mixing hot material into the photosphere faster than the CO↔CH_4 reaction can re-equilibrate (Hinz et al. 2010; Barman et al. 2011a). Similar but more extreme results have been found for 2MASS 1207 b, a 5–7 M_{jup} companion to a 25 M_{jup} TW Hya brown dwarf primary (Chauvin et al. 2004; Skemer et al. 2011; Barman et al. 2011b). Evidently, the HR 8799 planets and 2MASS 1207 b look similar to L-type brown dwarfs, despite having effective temperatures more consistent with T-type brown dwarfs.

Multiwavelength photometry and spectroscopy are the keys to understanding the differences between brown dwarfs and giant planets. In particular, working over a broad wavelength range is critical for understanding clouds, chemistry, and the radiative budget of extrasolar planets. The challenge of working over a broad wavelength range is that adaptive optics (AO) systems perform better at longer wavelengths where atmospheric turbulence is less severe. But background radiation increases at longer wavelengths, and most AO systems have numerous warm optics, which can make working at long wavelengths impractical (Lloyd-Hart 2000). The sweet spot for most AO systems has typically been the near-infrared (∼1–2.5 μm), although for extrasolar planets, there is a benefit to working at L' (3.8 μm), where the planet–star contrast improves (Heinze et al. 2008).

The Large Binocular Telescope (LBT) AO system can increase the wavelength range over which we study extrasolar planets. With its 672-actuator deformable secondary mirror (installed on one side of the telescope at the time of our observations), the system produces unprecedented image quality and contrast at short wavelengths. And because it is a deformable secondary AO system, it has a minimal number of warm optics, so that background noise remains low at long wavelengths.

In this paper, we present LBT First Light Adaptive Optics (FLAO) images of HR 8799 at H band (1.65 μm) and 3.3 μm, detecting the four planets (b–e) at both wavelengths. Both images are superior to previous attempts at these wavelengths due to the high performance of the LBT's AO system. Our images are the first detections of HR 8799 e at H band and 3.3 μm and the first unambiguous detections of HR 8799 b and d at 3.3 μm. In Section 2, we give a basic description of the instrumental setup for the FLAO system, the near-infrared imager, PISCES, and the mid-infrared imager, L- and M-band Infrared Camera (LMIRCam), which is a component of the Large Binoc-

ular Telescope Interferometer (LBTI). Additionally, we describe our data reduction procedure, which is an implementation of the Locally Optimized Combination of Images (LOCI) algorithm. In Section 3 we estimate photometry for the four planets, based on our LOCI reductions. In Section 4 we use our H-band image to search for additional companions interior to HR 8799 e, taking advantage of the unprecedented contrast afforded by the LBT AO system. In Section 5 we present thick-cloud, non-equilibrium chemistry model atmospheres and mixed-cloud atmospheres in an effort to explain the appearances of the HR 8799 planets. We conclude in Section 6 and make suggestions for future work characterizing HR 8799 and other directly imaged exoplanets. A companion paper, Esposito et al. (2012), describes the instrumental setup for the AO system and PISCES in detail, provides an independent analysis of the H-band data (along with new K_s-band data), and presents astrometry and a new orbital analysis of the system.

2. OBSERVATIONS

2.1. PISCES H Band

We observed HR 8799 at H band ($\lambda = 1.66$ μm; FWHM = 0.29 μm) with PISCES (McCarthy et al. 2001) on UT 2011 October 16, during Science Verification Time for the LBT FLAO system. The LBT's FLAO system (PI: Simone Esposito) is a 672-actuator deformable secondary AO system that makes use of an innovative pyramid wavefront sensor, producing high-Strehl-ratio, low-background images over a broad wavelength range (Esposito et al. 2010, 2011). At the time of our observations, one AO system was installed on the right telescope, so for the observations presented in this paper, only one 8.4 m mirror is used. PISCES (PI: Don McCarthy) is a 1–2.5 μm imager with a Hawaii 1024 × 1024 HgCdTe array, which at the LBT (single 8.25 m aperture) critically samples a diffraction-limited point-spread function (PSF) at H band (with a plate scale of 0″.0193 pixel^{-1}). For the observations in this paper, PISCES was installed on the front bent-Gregorian focus of the LBT's right side to take advantage of the LBT's new AO system, while facility infrared cameras are being delivered and commissioned.

During our H-band observations of HR 8799, conditions were photometric and the natural seeing, as measured by a differential image motion monitor (DIMM) on the telescope structure, was as good as ∼0″.9. We obtained 901 images with 2 s integrations, over the course of 2 hr (90° of sky rotation) with the telescope rotator turned off angular differential imaging (ADI; Marois et al. 2006). PISCES' readout time is 6 s, which means our observations were inefficient. However, high-contrast observations are usually limited by PSF stability rather than photon noise, so the long readouts had a negligible effect on our final results. The 2 s integrations saturated out to a radius of ∼0″.15. We were not able to obtain unsaturated H-band images of the star for photometry and astrometry with PISCES' shortest integration time, 0.8 s.

Images were processed to remove cross-talk and persistence as described in McCarthy et al. (2001) using the *corquad* correction software.[13] We then dark subtracted, flat fielded, and distortion corrected the images. Finally, images were aligned by maximizing their cross-correlation. We processed the aligned images using the LOCI algorithm (Lafrenière et al. 2007), which has been shown to produce higher contrast images than other algorithms, such as ADI. In the terminology of Lafrenière et al.
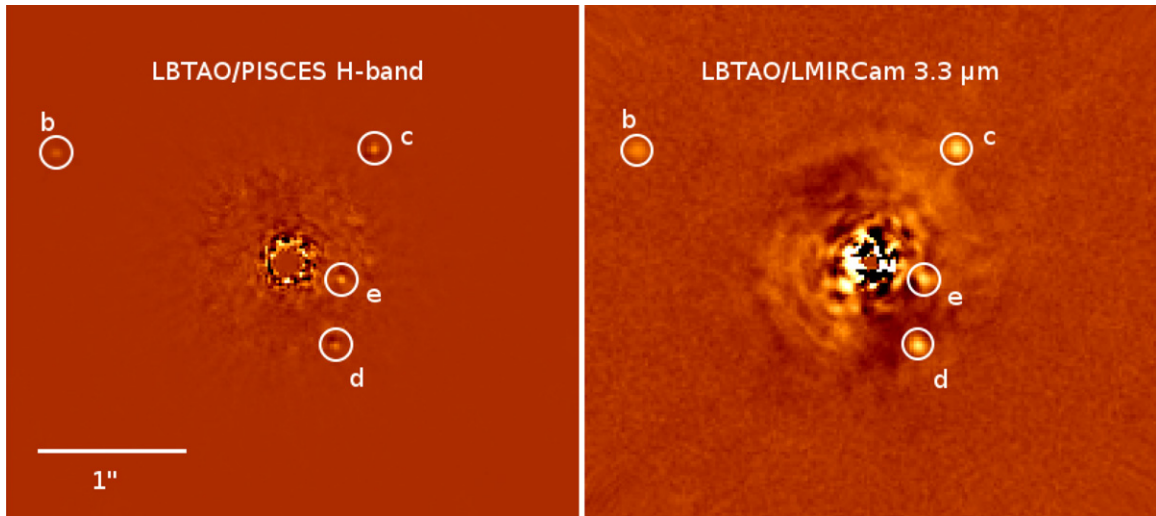
---

[13] http://aries.as.arizona.edu/~observer/dot.corquad.pisces

Figure 1. LBT First Light AO images of the HR 8799 planetary system at *H* band and 3.3 μm. These images constitute the first detection of HR 8799 e at either wavelength and the first unambiguous detections of HR 8799 b and d at 3.3 μm.

(A color version of this figure is available in the online journal.)

(2007), we used $N_\delta = 1$, $N_A = 300$, $g = 1$, and a 1 pixel subtraction region.[14] The values for N_A and g are adopted from Lafrenière et al. (2007), and we use $N_\delta = 1$ instead of $N_\delta = 0.5$ to suppress self-subtraction, although we note that changing N_δ to 0.5 has a negligible effect on our photometry. Our implementation of the LOCI algorithm also includes an FWHM-sized mask around every subtraction region to further suppress self-subtraction.

After reducing all 901 images with LOCI, we evaluated the noise of the images (standard deviation of pixel count) within an annulus from $0''\!.3$ to $0''\!.5$. The noise dramatically increased after the 500th image, corresponding to an increase in natural seeing. We reran LOCI using just the first 500 images (1000 s, 61° of sky rotation), marginally improving our final image, which is shown in Figure 1. HR 8799 b, c, d, and e are all clearly visible.

The LOCI algorithm assumes accurate knowledge of the star's position. However, the stellar core saturated even with PISCES' fastest readout. We were able to estimate the stellar centroid to within 0.5 pixels ($0''\!.01$) based on the circular symmetry of the PSF. We then reran LOCI with a set of different stellar centroid positions composing a 1×1 pixel box and found no significant astrometric or photometric discrepancies between the results.

2.2. LBTI/LMIRCam 3.3 μm

We observed HR 8799 at 3.3 μm ($\lambda = 3.31$ μm; FWHM = 0.40 μm) with LBTI/LMIRCam (Hinz et al. 2008; Skrutskie et al. 2010) on UT 2011 November 16. Although LBTI will eventually be used to combine the light from both LBT apertures, it was used in single-aperture mode for these observations, since only one AO system was operational. LBTI (PI: Phil Hinz) consists of a beam combiner (Universal Beam Combiner), which combines the light from the two telescope tertiary mirrors, and a science camera (Nulling Infrared Camera),

which itself contains a 2–5 μm channel (LMIRCam) and an 8–13 μm channel (Nulling Optimized Mid-Infrared Camera, NOMIC). LMIRCam uses a Hawaii 2RG 2048 × 2048 HgCdTe array, which oversamples $\lambda = 2$–5 μm PSFs (with a plate scale of $0''\!.0106$ pixel^{-1}) when using only one telescope primary.

Conditions during our 3.3 μm observations were photometric, with a natural seeing (as measured by the telescope DIMM) of $\sim 1''\!.1$. We obtained 1920 images with 3.8 s integrations over the course of 3.3 hr (110° of sky rotation). The 3.8 s exposure saturated inside of $0''\!.06$. We also obtained short (0.15 s) unsaturated images for astrometry/photometry. About 1% of the images had bad tip/tilt residuals and were removed.

Images were flat fielded, and globally bad pixels (defined as pixels further than 15% from the median flat) were replaced with the average of the eight nearest good pixels. The images were then nod subtracted with nods taken every 20 images. After these basic reduction steps, we found that some pixels had changing biases over shorter timescales than the nod subtraction. We removed these with three steps: subtracting the 3σ-clipped median of each column (to remove column bias-level effects), median-binning the data with a 2×2 box (since the PSF is oversampled by a factor of three for a single-aperture telescope), and replacing isolated bad pixels (4σ from their neighboring pixels) with the median of the neighboring pixels. For the remainder of this paper, LMIRCam "pixels" refer to binned pixels, which have a plate scale of $0''\!.0212$.

Images were processed with LOCI, using the same parameters and implementation described in Section 2.1. We evaluated the noise inside a $0''\!.2$–$0''\!.4$ annulus in each LOCI-processed image and removed $\sim 10\%$ of the images, which had high noise, due to residual bad pixels and/or sub-optimum AO performance. Our final image, which is shown in Figure 1, clearly shows planets b, c, d, and e.

3. PHOTOMETRY

Since LOCI self-subtracts, we calibrated our photometry by subtracting fake planets from the raw data at the positions of the detected planets and rerunning the full LOCI pipeline. Best-fit photometry and error bars were determined by adjusting the fluxes of the fake planets to determine the range of values resulting in reasonable subtractions. For the PISCES *H*-band

---

[14] The general idea of LOCI with ADI is as follows. The stellar PSF is removed in a set of subtraction regions, which together compose the image. For each subtraction region, the stellar PSF is estimated by constructing a linear combination of individual exposures that minimizes noise within a corresponding optimization region, which is centered on the subtraction region but is much larger. The optimization region is an annulus with an area of N_A PSF cores and a ratio between its radial extent and azimuthal extent of g. Images whose parallactic angle differs by less than an amount such that a source would move by N_δ FWHM are excluded from the optimization.

Table 1
LBT Photometry of the HR 8799 Planets

Planet	ΔH Mag with HR 8799 b	Absolute H Mag	$\Delta 3.3$ μm Mag with HR 8799	Absolute 3.3 μm Mag
HR 8799 b		$15.08 \pm 0.13^{\mathrm{a}}$	10.97 ± 0.10	13.22 ± 0.11
HR 8799 c	-0.90 ± 0.05	14.18 ± 0.14	9.97 ± 0.10	12.22 ± 0.11
HR 8799 d	-0.85 ± 0.2	14.23 ± 0.2	9.77 ± 0.10	12.02 ± 0.11
HR 8799 e	-1.2 ± 0.2	13.88 ± 0.2	9.87 ± 0.20	12.02 ± 0.21

Notes. [a] HR 8799 b absolute H-band photometry from Metchev et al. (2009). Absolute H-band photometry for the other planets is with respect to HR 8799 b.

data, the star was saturated, so we calculated photometry for planets c, d, and e with respect to HR 8799 b and converted to absolute magnitudes by adopting the magnitude of HR 8799 b from Metchev et al. (2009). For the LMIRCam 3.3 μm data, we calculated photometry for all four planets with respect to unsaturated images of the star, obtained immediately after the saturated images used to detect the planets. We converted these to absolute photometry using HR 8799's absolute magnitude at 3.3 μm from Hinz et al. (2010). Errors on the LMIRCam absolute calibration are primarily the result of changing Strehl ratios and telluric absorption variation throughout our observations. To test the magnitude of the Strehl-ratio variation, we performed $r = \lambda/D$ aperture photometry on the unsaturated data and found a standard deviation of only ∼2%. To test the magnitude of the telluric absorption variation, we compared the Airy pattern of the saturated and unsaturated images and found them to be consistent within ∼5%. Combining these error terms, we adopt an absolute calibration error of 0.06 mag for the LMIRCam 3.3 μm data. H-band and 3.3 μm photometry of HR 8799 is presented in Table 1.

Our H-band photometry for HR 8799 c and d is consistent with the results of Marois et al. (2008) and Metchev et al. (2009), and we detect HR 8799 e for the first time at H band, finding it to be ∼0.3 mag brighter than the next brightest planet (HR 8799 c). Our 3.3 μm data are somewhat inconsistent with previous photometry from Hinz et al. (2010) and Currie et al. (2011), which are independent reductions of observations taken with MMT/Clio (note that the Clio and LMIRCam 3.3 μm filters are identical). Hinz et al. (2010) reported detections of HR 8799 c and d but not b, and Currie et al. (2011) reported detections of HR 8799 b and c but not d. The most substantial disparity is for HR 8799 b, for which Hinz et al. (2010) reported an absolute magnitude upper limit of 14.82, while Currie et al. (2011) reported a detection of 13.96 ± 0.28. Our detection of 13.22 ± 0.11 is closer to the result of Currie et al. (2011) but is still brighter by a significant amount. We reanalyzed the final reduced images from Hinz et al. (2010) and find the upper limit reported by Hinz et al. (2010) to be erroneous (likely a typographic error). Our photometry for HR 8799 c is also brighter than observed by Hinz et al. (2010) and Currie et al. (2011), and our photometry of HR 8799 d is brighter than observed by Hinz et al. (2010). We present a comparison of the MMT/Clio image and our new LBT/LMIRCam image in Figure 2. The fact that our photometry is somewhat inconsistent with the values of Hinz et al. (2010) and Currie et al. (2011) can likely be explained by the non-photometric conditions reported in Hinz et al. (2010), varying AO performance (caused by the non-photometric conditions) and overly optimistic systematic and/or measurement error analyses considering the quality of the Clio data. Variability is unlikely to be a factor, given that it has not been reported in any other photometric band and the amplitude of variability needed to rectify the disparity is quite large.

4. CONSTRAINTS ON A HYPOTHETICAL FIFTH PLANET, HR 8799 f

While HR 8799 is known to have four giant planets at wide separations, the inner system might have one or more companions that have not yet been discovered. Additional companions would challenge formation models, which already have a hard time explaining the outer four planets (Dodson-Robinson et al. 2009; Kratter et al. 2010). A fifth planet would also complicate dynamical stability analyses, which require mean-motion resonances and planet masses that are on the low end of the range predicted by evolutionary models and independent age estimates (Fabrycky & Murray-Clay 2010; Moro-Martín et al. 2010; Sudol & Haghighipour 2012). Hinkley et al. (2011) used non-redundant masking to rule out the presence of massive inner companions from ∼0''.01 to 0''.5, but only for objects significantly more massive than the four known planets. Here we use our H-band image to search for planetary mass companions interior to HR 8799 e.

We evaluate our ability to detect a close-in companion by making a contrast curve of our residual H-band image (after the four planets have been removed).[15] We smooth the image with a Gaussian that is the same size as our diffraction-limited PSF and calculate the standard deviation in 1 pixel annuli. Counts are converted to photometry using the peak-flux (central pixel) of planet "b" from the smoothed image. We also correct for self-subtraction, which is measured by inserting fake planets into the raw data at various radii. Our 5σ contrast curve is shown in Figure 3. HR 8799 b–e are shown as diamonds. The vertical dashed line denotes the separation of the 2:1 mean-motion resonance with HR 8799 e (assuming a face-on circular orbit for simplicity). If there is a massive interior planet, it is likely to be in a stable resonance, as has been found for pairs of the outer four planets. We find no fifth planet at or exterior to the 2:1 resonance with HR 8799 e, with limits down to the approximate brightnesses (and by extension, masses) of the inner three planets. As a check, we insert a fake "e"-like planet into our raw images at a separation of 0''.235, the approximate position of the 2:1 resonance with "e." Our reduced image (Figure 4) shows that we would have detected "planet f" anywhere exterior to the 2:1 resonance, and that there are no residuals brighter than "f" in the image. Note that we do not repeat this analysis with the 3.3 μm image because it is not as sensitive to additional companions as the H-band image.

---

[15] Note that we use an H-band image constructed with $N_\delta = 0.5$ instead of $N_\delta = 1.0$ (which was described in Section 3) to maximize signal-to-noise ratio, as described in Lafrenière et al. (2007). The $N_\delta = 0.5$ contrast curve is ∼0.1–0.2 mag better than the $N_\delta = 1.0$ contrast curve from ∼0''.2 to 0''.3 and then becomes progressively worse (up to ∼0.5 mag) outside of 0''.3. For this section, the inner regions are more important, so we use the $N_\delta = 0.5$ contrast curve.
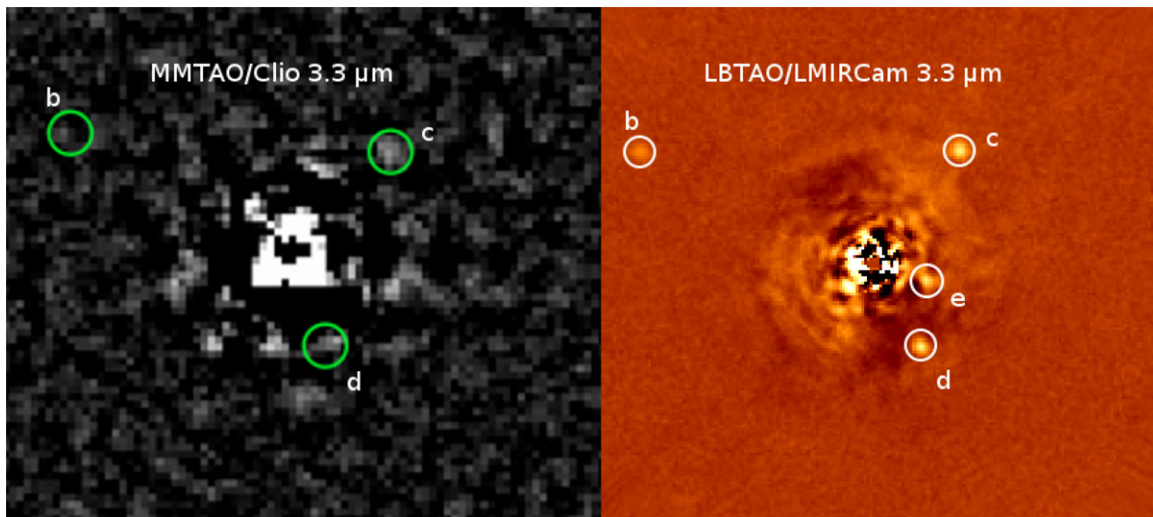
Figure 2. Comparison of the MMTAO/Clio 3.3 μm image from Hinz et al. (2010) and our new LBTAO/LMIRCam 3.3 μm image. Our 3.3 μm photometry is somewhat inconsistent with the findings of Hinz et al. (2010) and Currie et al. (2011), who separately analyzed the MMT data. Based on the relative quality of the images, it is likely that the disparity is the result of overly optimistic error bars by Hinz et al. (2010) and Currie et al. (2011).
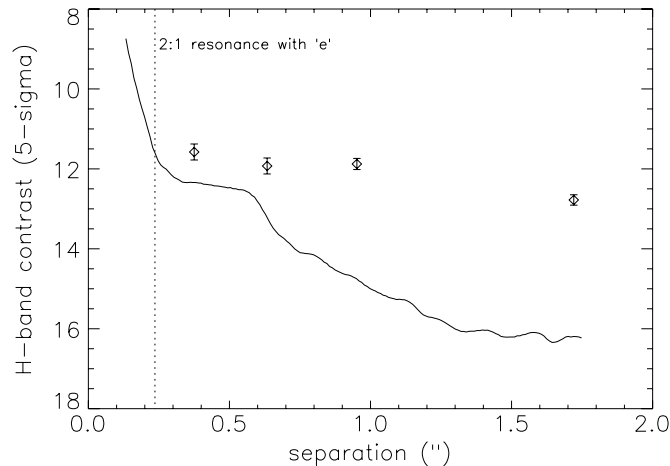(A color version of this figure is available in the online journal.)

Figure 3. H-band contrast curve for the LBTAO/PISCES H-band image of HR 8799, with the four planets shown. Also shown is the position of the 2:1 orbital resonance with HR 8799 e (assuming, for simplicity, a face-on, non-eccentric orbit). If there is a massive inner planet, it is likely to be in a stable resonance, as has been found for the outer companions. Based on the contrast curve, we would have been able to detect a planet at HR 8799 e's 2:1 inner resonance, if it were approximately as bright (massive) as HR 8799 cde. Note that the contrast curve shows a dark hole inside of ∼0″.6, which is a predicted feature of high-order adaptive optics systems (Malbet et al. 1995).
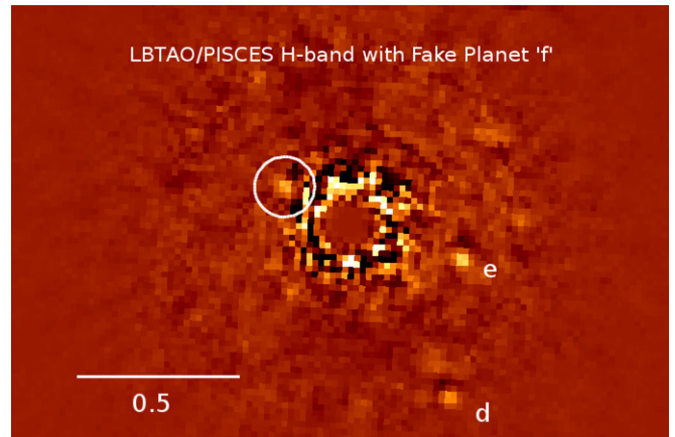

Figure 4. Image of the HR 8799 system with a fake planet, "f," added in at the approximate location of HR 8799 e's 2:1 orbital resonance. The fake planet, which is the same brightness as HR 8799 e, was added into our individual raw frames and is easily recovered by our LOCI pipeline. There are no residual point sources as bright as the fake planet at or exterior to its position at the HR 8799 e 2:1 orbital resonance.
(A color version of this figure is available in the online journal.)

5. MULTIWAVELENGTH MODELING OF THE HR 8799 PLANETS

Multiwavelength photometry and spectroscopy have improved our understanding of the physical properties of the HR 8799 planets, which are not well fit by the same models that have been used to interpret the properties of field brown dwarfs. Marois et al. (2008) first noted that the HR 8799 planet spectral energy distributions (SEDs) were best fit by model atmospheres with $T = 1400$–1700 K, while their luminosities were more consistent with $T = 800$–1000 K. The disparity was driven by the planets' faint/red appearance with respect to models and a lack of methane absorption in narrowband 1.59/1.68 CH_4 photometry. Subsequent 3.88–4.10 μm spectroscopy of HR 8799 c was inconsistent with both COND (Baraffe et al.

2003) and DUSTY (Chabrier et al. 2000) atmospheric models, which the authors interpreted as evidence for non-equilibrium chemistry (Janson et al. 2010). Three-color photometry in the L and M bands was also inconsistent with equilibrium chemistry atmospheric models and, in particular, showed a relative lack of methane absorption at 3.3 μm (Hinz et al. 2010). H and K spectroscopy of HR 8799 b also showed a methane deficiency (Bowler et al. 2010; Barman et al. 2011a). Currie et al. (2011) and Madhusudhan et al. (2011) were able to parameterize thick-cloud models to fit multiwavelength photometry for HR 8799 bcd. However, the models were not able to reproduce the 3.3 μm photometry or the subsequent spectroscopy of Barman et al. (2011a), who fit both the photometry and spectroscopy of HR 8799 b with models that incorporated clouds and non-equilibrium chemistry.

The combined result of these studies is that HR 8799 b, c, and d have non-equilibrium CO↔CH_4 chemistry and cloudy
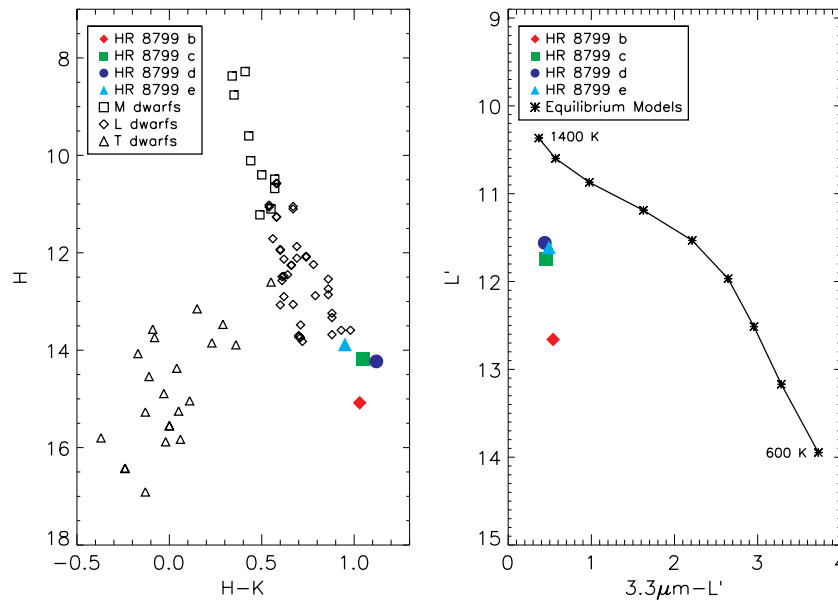
Figure 5. Left: H vs. $H-K$ color–magnitude diagram showing the M→L→T spectral-type transition for field brown dwarfs (Leggett et al. 2002; Knapp et al. 2004) and the HR 8799 planets. The HR 8799 planets appear to be an extension of the L-dwarf sequence, implying that they have cloudy atmospheres at lower effective temperatures than are typical for cloudy field brown dwarfs. Right: L' vs. $3.3\,\mu$m$-L'$ color–magnitude diagram showing equilibrium chemistry, thick-cloud atmospheres from Madhusudhan et al. (2011), and the HR 8799 planets. The HR 8799 planets are all brighter at $3.3\,\mu$m than predicted by the Madhusudhan et al. (2011) models, implying a lack of CH_4, which is a strong absorber at $3.3\,\mu$m in the equilibrium chemistry model atmospheres.

(A color version of this figure is available in the online journal.)

Table 2
Photometry of the HR 8799 Planets

Planet	z ($1.03\,\mu$m)	J ($1.25\,\mu$m)	H ($1.63\,\mu$m)	CH_4s ($1.59\,\mu$m)	CH_4l ($1.68\,\mu$m)	K_s ($2.15\,\mu$m)	3.3 ($3.3\,\mu$m)	L' ($3.8\,\mu$m)	M ($4.7\,\mu$m)
HR 8799 b	18.24 ± 0.29	16.30 ± 0.16	15.08 ± 0.13	15.18 ± 0.17	14.89 ± 0.18	14.05 ± 0.08	13.2 ± 0.11	12.66 ± 0.11	13.07 ± 0.30
HR 8799 c		14.65 ± 0.17	14.18 ± 0.14	14.25 ± 0.19	13.90 ± 0.19	13.13 ± 0.08	12.2 ± 0.11	11.74 ± 0.09	12.05 ± 0.14
HR 8799 d		15.26 ± 0.43	14.23 ± 0.2		14.03 ± 0.30	14.57 ± 0.23	13.11 ± 0.12	12.0 ± 0.11	11.56 ± 0.16	11.67 ± 0.35
HR 8799 e			13.88 ± 0.2			12.93 ± 0.22	12.1 ± 0.21	11.61 ± 0.12	
Reference (b,c,d,e)	2	3,3,3	4,1,1,1	3,3,3	3,3,3	3,3,3,5	1,1,1,1	3,3,3,5	6,6,6

References. (1) This work; (2) Currie et al. 2011; (3) Marois et al. 2008; (4) Metchev et al. 2009; (5) Marois et al. 2010; (6) Galicher et al. 2011.

atmospheres at low effective temperatures where, in field brown dwarfs, the clouds are thought to have settled below the photosphere. Two color–magnitude diagrams, shown in Figure 5, demonstrate these effects. On the left is an $H-K$ versus H color–magnitude diagram, which shows the M→L→T sequence of field brown dwarfs. L dwarfs are characterized by cloudy atmospheres, while T dwarfs are characterized by cloud-free atmospheres. The intermediate region is the L→T transition, where objects are thought to have patchy clouds or clouds that have partially descended below the photosphere. The HR 8799 planets appear to be an extension of the field L-dwarf sequence, i.e., they have clouds at an effective temperature where the field brown dwarfs are transitioning to cloudless. The right-hand side of Figure 5 shows a $3.3\,\mu$m$-L'$ versus L' color–magnitude diagram, which includes a sequence of chemical equilibrium, thick-cloud models from Madhusudhan et al. (2011). The HR 8799 planets are all much brighter at $3.3\,\mu$m than predicted by the models, implying a relative absence of CH_4, which is a strong absorber at $3.3\,\mu$m.

In the following sections, we present model atmospheres of the HR 8799 planets in an attempt to reproduce their photometry. A summary of the available photometry is presented in Table 2, colors are presented in Table 3, and a listing of all the models used in this paper is presented in Table 4. For

Table 3
Colors of the HR 8799 Planets

Planet	$J-H$	$H-K_s$	K_s-L'	$3.3\,\mu$m$-L'$	$L'-M$
HR 8799 b	1.22 ± 0.20	1.03 ± 0.15	1.39 ± 0.13	0.54 ± 0.15	-0.41 ± 0.31
HR 8799 c	0.47 ± 0.21	1.05 ± 0.16	1.39 ± 0.12	0.46 ± 0.14	-0.31 ± 0.16
HR 8799 d	1.03 ± 0.46	1.12 ± 0.23	1.55 ± 0.20	0.44 ± 0.19	-0.11 ± 0.37
HR 8799 e		0.95 ± 0.29	1.32 ± 0.25	0.49 ± 0.24	

all model comparisons in this paper, we convolve the model planet atmosphere and a model of Vega (Cohen et al. 1992) with filter profiles to produce predicted magnitudes in the different filters, which are then compared to the measured photometry. The filter profiles have all been multiplied by a model telluric atmosphere.[16] For most filters, this step has a negligible effect, because the telluric atmosphere has a flat transmission profile, but Earth's atmosphere has a large transmission slope in the $3.3\,\mu$m filter that changes the effective wavelength of the filter and, in turn, changes the model magnitudes by ∼0.1 mag. For the sake of plotting the model fits, we convert the filter magnitudes to Jy by convolving the Vega model with filter profiles to

---

[16] http://www.gemini.edu/sciops/ObsProcess/obsConstraints/atm-models/cptrans_zm_43_15.dat

Table 4
Atmospheric Models Used in This Paper

Figure No.	$T_{\rm eff}$ (K)	$\log(g)$	Cloud Type	Chemistry
6	850	4.3	AE.60	Equilibrium
				$10 \times CO, 0.1 \times CH_4$
				$100 \times CO, 0.01 \times CH_4$
7	1400	4.0	AE.60	Equilibrium
	700		A.100	
8	1000	4.2	AE.60	Equilibrium
				$10 \times CO, 0.1 \times CH_4$
				$100 \times CO, 0.01 \times CH_4$
	900	3.8	AE.60	Equilibrium
				$10 \times CO, 0.1 \times CH_4$
				$100 \times CO, 0.01 \times CH_4$
9	1400	4.0	AE.60	Equilibrium
	700		A.100	
10	1000	4.0	AE.60	Equilibrium
11	1000	4.0	AE.60	Equilibrium
				$10 \times CO, 0.1 \times CH_4$
				$100 \times CO, 0.01 \times CH_4$
12	1400	4.0	AE.60	Equilibrium
	700		A.100	

Notes. Cloud types ("A" and "AE") refer to cloud thickness, and the associated numbers ("60" and "100") refer to modal dust grain size, as parameterized in Madhusudhan et al. (2011). Multiples of CO and CH_4 are with respect to equilibrium chemistry models. All models assume solar metallicity. Further model details are discussed in Burrows et al. (2006) and Madhusudhan et al. (2011).

produce zero-point fluxes. For HR 8799 b, we also include the H and K spectroscopy from Barman et al. (2011a). The HK spectrum comparison is made by smoothing the planet model atmosphere by the published spectrum's resolution (0.01 μm) and directly comparing to the observed spectrum. The absolute fluxes of the H and K spectroscopy are tied to the H and K photometry, so for our comparison we allow the overall brightness of the two spectra to vary and only fit the shapes of the spectra.

5.1. HR 8799 b

HR 8799 b is the most challenging atmosphere to explain because it is the coolest of the four planets and is thus the largest outlier in the color–magnitude diagrams shown in Figure 5. Additionally, the HR 8799 b atmosphere is the most constrained of the four planets due to the H and K spectroscopy of Barman et al. (2011a). Our new 3.3 μm photometry of HR 8799 b is significantly brighter (by ~100%) than the previously published value by Currie et al. (2011). As described in Section 3, the Currie et al. (2011) 3.3 μm photometry is likely erroneous, due to non-photometric conditions and/ory overly optimistic error bars. There is the possibility that HR 8799 b is extremely variable at 3.3 μm, but we consider that scenario unlikely due to the many times HR 8799 has been observed at other wavelengths where there has been no evidence of such large variability.

Before proceeding with our modeling, we examine Barman et al.'s (2011a) recent hypothesis regarding the SED of HR 8799 b. Barman et al. (2011a) were able to reproduce all existing photometry and spectroscopy of HR 8799 b by using a non-equilibrium CO↔CH$_4$ cloudy atmosphere with $T_{\rm eff} = 1100$ K and $\log(g) = 3.5$. However, their model is inconsistent

with interior evolutionary models, which predict a larger object radius. Barman et al. (2011a) also present model atmospheres that obey the predictions of the evolutionary tracks, with a best-fit model that has $T = 896$ K and $Z = 1.0$ metallicity. This model demonstrates that it might be possible to explain HR 8799 b's appearance with a combination of clouds, non-equilibrium chemistry, and higher than solar metallicity. However, the model does not fit all of the existing photometry, and our new 3.3 μm photometry makes the fit significantly worse.

5.1.1. Non-equilibrium CO↔CH$_4$ Chemistry

We start our modeling by using the parameterized thick-cloud atmospheres of Madhusudhan et al. (2011) and adjusting the CO and CH$_4$ mixing ratios. These models assume evolutionary track radii but make no attempt to self-consistently explain the CO and CH$_4$ mixing ratios, which Barman et al. (2011a) produce with turbulent mixing. In Figure 6, we plot the best-fit chemical equilibrium model of HR 8799 b from Madhusudhan et al. (2011), as well as two models that have suppressed CH$_4$ and enhanced CO with respect to the equilibrium models (by factors of 10 and 100, respectively). Suppressing CH$_4$ and enhancing CO has a negligible effect on the near-infrared ($zJHK$) photometry, but it greatly affects the HK spectroscopy, favoring the $100 \times$CO, $0.01 \times$CH$_4$ model. Non-equilibrium chemistry dramatically affects the 3–5 μm SED, where a lack of CH$_4$ makes the object brighter in the 3.3 μm and L' filters and excess CO makes the object fainter in the M-band filter. The $100 \times$CO, $0.01 \times$CH$_4$ model fits the 3.3 μm photometry and comes closest to fitting the M-band photometry (further increasing the CO mixing ratio would improve this fit). However, the lack of CH$_4$ strongly increases the predicted flux in the L' filter, making it incompatible with HR 8799 b's observed L' photometry. Based on this analysis, it seems unlikely that a cool (850 K) atmosphere with non-equilibrium chemistry could explain HR 8799 b's 3.3 μm$-L'$ color. However, there remains the possibility that more complex radial profiles of non-equilibrium chemistry and clouds could explain all of the data.

5.1.2. Mixed-cloud Atmospheres

Based on Figure 5, HR 8799 b has colors reflective of a ~1300 K atmosphere, but a luminosity consistent with an ~850 K atmosphere. In lieu of resolving the difference by assuming a small (unphysical) radius, we consider the possibility that the planet emits non-isotropically, with bright and dark sections, such that the bright sections dominate the shape of the SED. Bright and dark regions have been observed on Jupiter in the mid-infrared (Westphal 1969), and several studies seeking to explain the L→T transition have used hybrid cloudy/cloud-free models (e.g., Burgasser et al. 2002). For our purposes, mixtures of standard cloudy and cloud-free models are unlikely to explain the appearance of HR 8799 b because its $H - K$ color is redder than the L-dwarf sequence, implying that it is more cloudy, not less cloudy, than the other L dwarfs.

An alternative is that HR 8799 b has a mixture of clouds, such that the whole planet is cloudy, but with regions that have thicker clouds where the planet appears darker. A coarse approximation of this phenomenon is to linearly combine cloudy models of different effective temperatures (analogously to how Burgasser et al. 2002 and others have linearly combined cloudy and cloud-free models of different effective temperatures). This method is somewhat non-physical due to the fact that the two atmospheres have different temperature–pressure
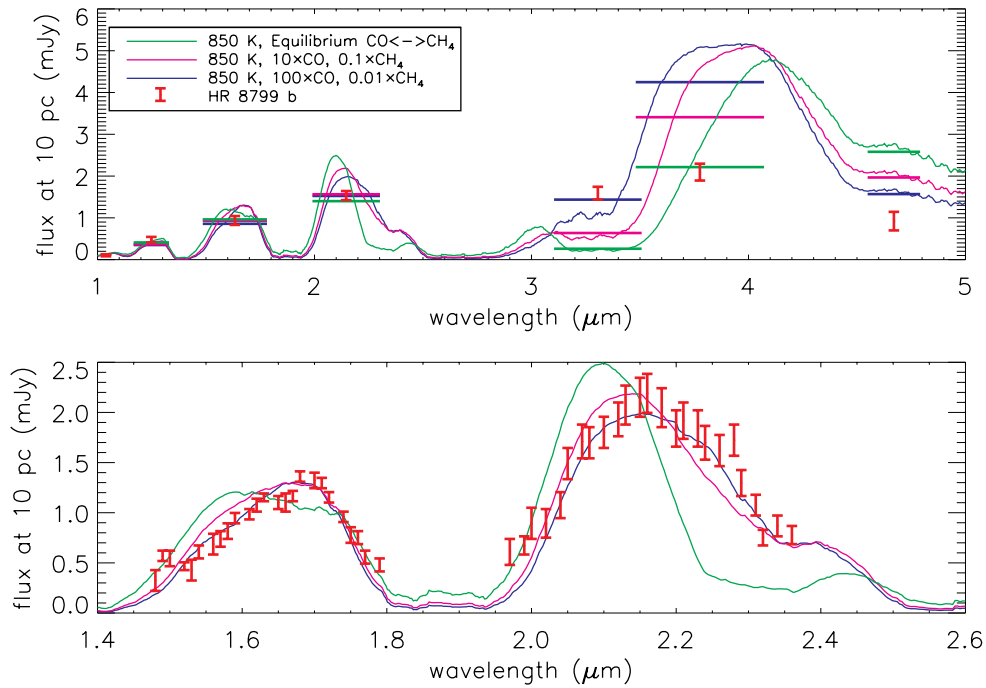
Figure 6. Photometry and spectroscopy of HR 8799 b (red error bars; Table 2 and Barman et al. 2011a) with atmospheric models (green, pink, and blue curves) and predicted in-band fluxes for each photometry point (green, pink, and blue horizontal lines, which span the filters' half-max profiles). The 850 K equilibrium chemistry model (green) is the best-fit "thick-cloud" model for HR 8799 b from Madhusudhan et al. (2011). Two other models (pink and blue) suppress the CH_4 mixing ratios and enhance the CO mixing ratios by 10× and 100× with respect to the equilibrium chemistry model. The H and K spectroscopy are well fit by the non-equilibrium chemistry models. Our new 3.3 μm photometry is best fit by the 100×CO, 0.01×CH_4 model. However, this model predicts a flux that is substantially higher than published measurements at 3.8 μm (L'). None of the models are able to reproduce the relatively flat SED from 3.3 to 3.8 μm.

(A color version of this figure is available in the online journal.)
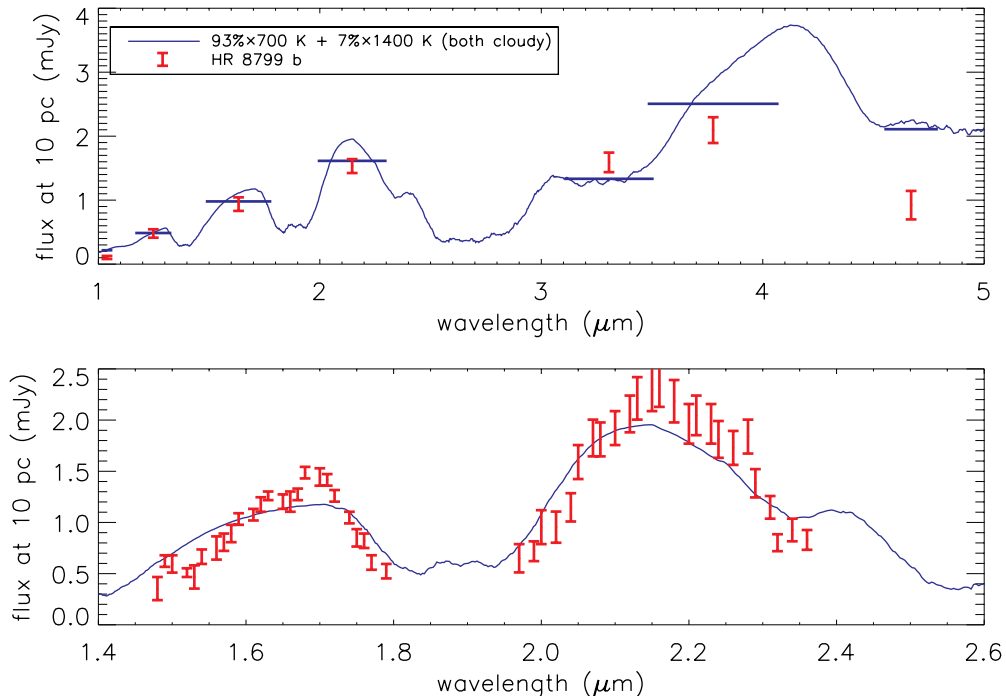
Figure 7. Same as Figure 6 but with a mixed-cloud model (93% 700 K A-type clouds and 7% 1400 K AE-type clouds from Madhusudhan et al. 2011). The fit adequately reproduces all photometry (except in the M-band filter, where additional CO absorption would rectify the discrepancy) and greatly flattens the SED from 3.3 to 3.8 μm compared to the non-equilibrium models shown in Figure 6. At H and K, the model generally reproduces the shape of HR 8799 b's observed spectrum (i.e., negligible CH_4 absorption) but is flatter.

(A color version of this figure is available in the online journal.)

profiles (Marley et al. 2010). Linearly combining models with a shared temperature–pressure profile but different cloud structures would be more correct but is beyond the scope of this

paper. In Figure 7, we present an example of a hybrid atmosphere that is 93% $T_{\rm eff} = 700$ K, "A"-type cloudy and 7% $T_{\rm eff} = 1400$ K, "AE"-type cloudy (A and AE cloud profiles
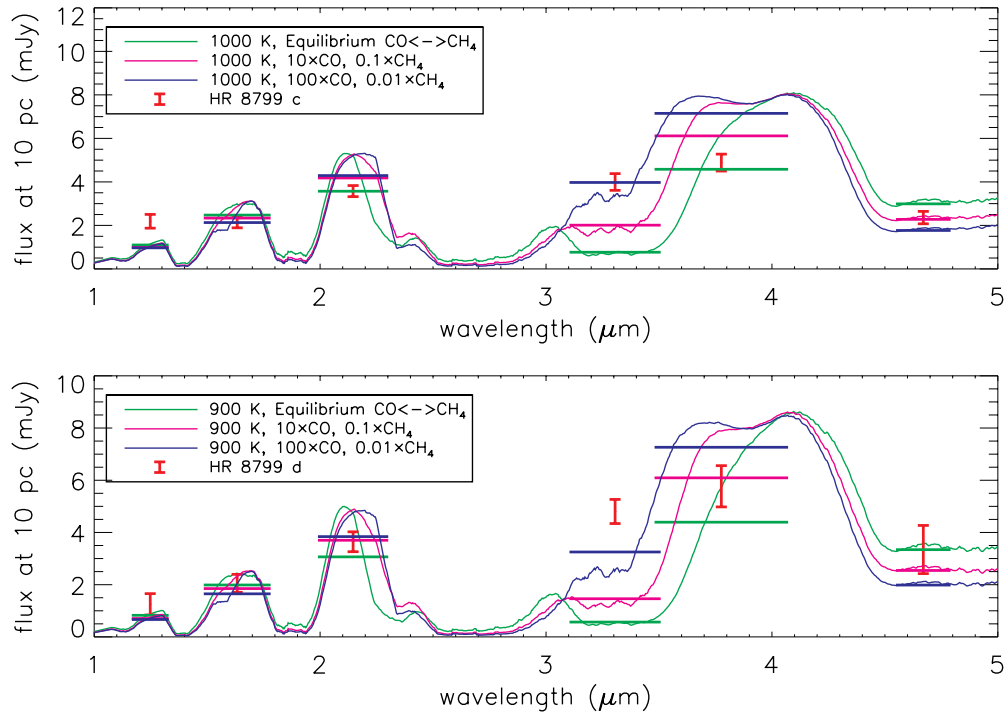
Figure 8. Same as Figure 6 (top) but for HR 8799 c and d. As was found for HR 8799 b, our non-equilibrium chemistry models are unable to fit the 3.3 μm$-L'$ colors of HR 8799 c and d.

(A color version of this figure is available in the online journal.)
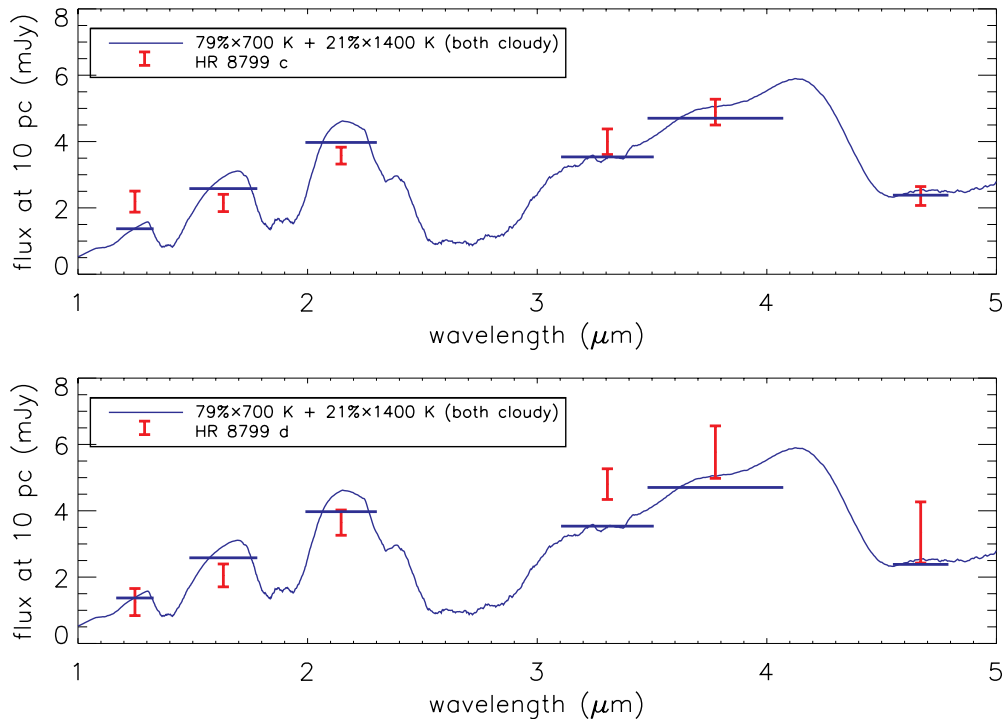

Figure 9. Same as Figure 7 (top) but for HR 8799 c and d. We purposely choose the same cloudy atmospheres to mix as were used for HR 8799 b. We are able to fit HR 8799 c and d with mixed-cloud atmospheres, but using a higher mixing fraction of the 1400 K atmosphere than was found for HR 8799 b. The addition of non-equilibrium chemistry to these models would likely improve the fit.

(A color version of this figure is available in the online journal.)

are described in Madhusudhan et al. (2011), and further model details are presented in Burrows et al. 2006). The hybrid model adequately fits all of the photometry except for *M* band, which can be explained with further increased CO absorption. The *HK* model spectrum is muted compared to the data,

but its bulk shape is generally correct (i.e., it does not show strong CH$_4$ absorption, as would be expected for a cool object). We note that this model is meant to be representative, but that a true mixed-cloud atmosphere should be calculated self-consistently.
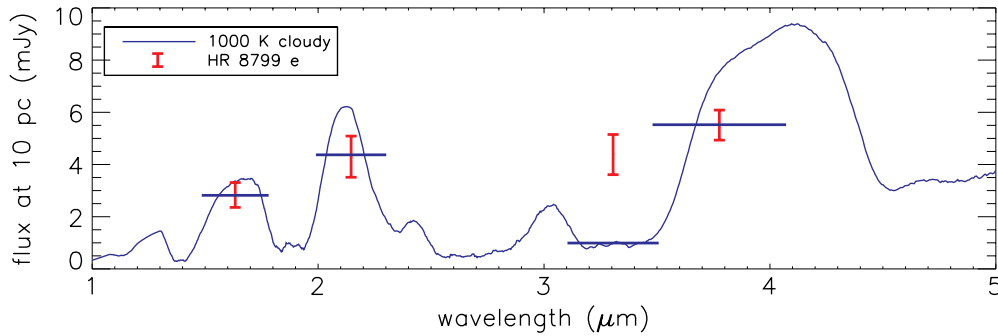
Figure 10. Thick-cloud atmosphere for HR 8799 e (plotted with the same symbols used in Figures 6–9). In this fit, we ignore the 3.3 μm photometry as was done by Madhusudhan et al. (2011) when fitting HR 8799 b, c, and d.

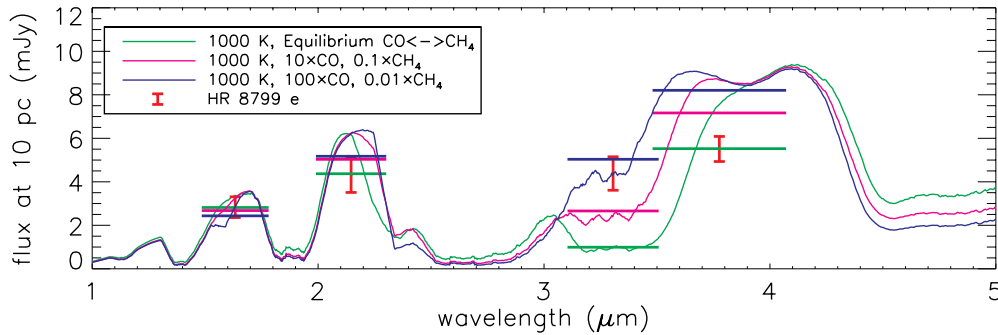(A color version of this figure is available in the online journal.)

Figure 11. Same as Figures 6 (top) and 8 but for HR 8799 c and d. As was found for HR 8799 b, c, and d, our non-equilibrium chemistry models are unable to fit the 3.3 μm−L' colors of HR 8799 e.

(A color version of this figure is available in the online journal.)

5.2. HR 8799 c, d, and e

We repeat our analysis of HR 8799 b (Section 5.1) for HR 8799 c and d, again starting with the best-fit, thick-cloud models from Madhusudhan et al. (2011). A comparison of non-equilibrium CO↔CH$_4$ models is shown in Figure 8, and example mixed-cloud atmospheres are shown in Figure 9. Our conclusions for HR 8799 c and d are similar to our conclusions for HR 8799 b: we are unable to fit the 3.3 μm−L' colors of HR 8799 c and d with cloudy/non-equilibrium chemistry models, and mixed-cloud atmospheres do a reasonable job fitting all of the data. We purposely construct the mixed-cloud atmospheres from the same two model atmospheres used to make the mixture for HR 8799 b (see Section 5.1.2). In this scenario, we find that HR 8799 c and d have higher fractions of the warm atmosphere than HR 8799 b, explaining their higher luminosity.

HR 8799 e has less data than the outer three planets, but the existing data are consistent with the photometry of HR 8799 c and d. With the addition of our new H-band and 3.3 μm photometry, HR 8799 e has now been studied at four wavelengths, and we can proceed with atmospheric modeling, based on lessons learned from HR 8799 b, c, and d. We begin by using the thick-cloud models from Madhusudhan et al. (2011) to look for a good fit of the H, K, and L' photometry. We find that a 1000 K, log(g) = 4.0 model fits well (shown in Figure 10). Based on the small number of data points, degeneracies between different cloud properties, surface gravity, and effective temperature are not explored, but it is reasonable to assume that the cloud properties and surface gravity will be similar to the other HR 8799 planets. Figures 11 and 12 show non-equilibrium chemistry models and mixed-cloud models. As was true for the outer three planets, we are unable to fit the

available photometry with non-equilibrium chemistry models, and a mixed-cloud model can be made to fit.

5.3. The HR 8799 Planets in Aggregate

The HR 8799 system provides a unique laboratory for simultaneously studying multiple coeval planets. In the previous sections, we have modeled the planets individually. Comparing the four planets provides additional insight.

HR 8799 c, d, and e are brighter than HR 8799 b in all published photometry but have almost exactly the same colors as "b" throughout their measured SEDs (see Table 3; the colors for all four planets are the same, within errors, except for $J − H$ for HR 8799 c, where J is abnormally bright). Given that the planets are coeval, they are expected to all have similar radii (to within ∼10%; Burrows et al. 1997). Therefore, the fact that "c," "d," and "e" are brighter than "b" implies that they have higher effective temperatures (based on $L = 4\pi R^2 \sigma T_{\rm eff}^4$). However, the fact that all of the HR 8799 planets have the same colors suggests that the physical properties of their atmospheres are similar, despite their different effective temperatures. In field brown dwarfs, objects with different effective temperatures (over the range probed by the HR 8799 planets) have different physical properties and different SED colors. For the HR 8799 planets, this does not appear to be the case.[17]

The fact that "c," "d," and "e" have almost the exact same colors as "b" is circumstantial evidence for the mixed-cloud atmospheres. In the mixed-cloud scenario, HR 8799 b has a lower *effective* temperature than the other HR 8799 planets, but

_____

[17] As an example, Dupuy & Liu (2012) find $\Delta K − L'/\Delta K = 0.4$ over a large effective temperature range, whereas HR 8799 b has a $\Delta K − L'/\Delta K = 0.03$ with respect to the average values of HR 8799 c, d, and e.
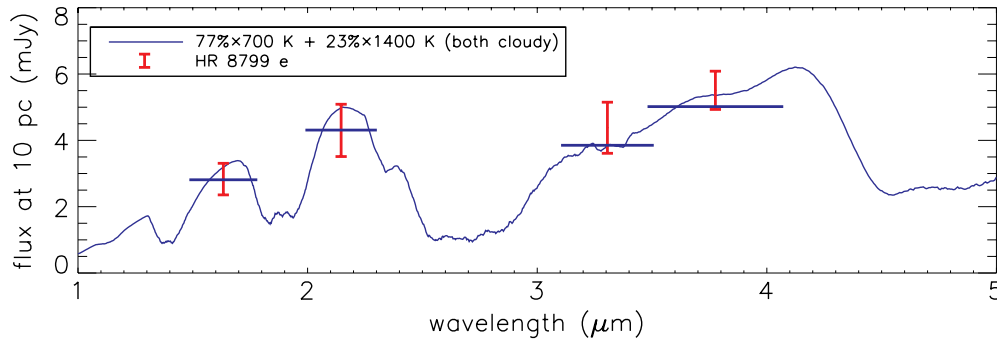
Figure 12. Same as Figures 7 (top) and 9 but for HR 8799 e. The mixing fraction of the two atmospheres is similar to what we found for HR 8799 c and d. The addition of non-equilibrium chemistry to these models would slightly improve the fit, although the photometric error bars for HR 8799 e are large enough that this is not necessary.

(A color version of this figure is available in the online journal.)

a similar *physical* temperature in the bright, emitting regions of its atmosphere. In Figures 7, 9, and 12, we have shown that all of the HR 8799 planets can be fit by a mixture of 1400 K and 700 K cloudy atmospheres (which we have been using as an approximation for two different cloud structures, one of which has much lower opacity). The difference between the cooler planet, "b," and the hotter planets, "c," "d," and "e," is the mixing ratio of the 1400 K and 700 K models, i.e., the covering fraction of the different cloud types.

The non-equilibrium chemistry models (with reasonable radii) of Barman et al. (2011a) fit the *HK* spectroscopy better than our makeshift mixed-cloud models, but they do not reproduce the broadband colors as well, in particular from 3.3 to 3.8 μm. The Barman et al. (2011a) models do provide physical motivations for non-equilibrium chemistry (turbulent radial mixing), while our mixed-cloud models are based on analogy with physically quite different systems (Jupiter and L/T transition brown dwarfs). Self-consistent modeling is still necessary to determine if mixed-cloud atmospheres are a viable explanation for the HR 8799 planets. In any case, it appears that detailed modeling of increasingly complex cloud physics and chemistry will be necessary to explain the true nature of the HR 8799 planets.

6. SUMMARY AND CONCLUSIONS

We have directly imaged the HR 8799 planetary system, detecting all four planets at *H* band and 3.3 μm with the LBT's FLAO system. The images are of unprecedented quality, allowing us to rule out the presence of a massive (HR 8799 cde-like) planet exterior to HR 8799 e's 2:1 inner resonance (*H* band 5σ contrast of 11.6 mag at 0.″235). We detect HR 8799 e at *H* band, for the first time, and find that it is approximately as bright as HR 8799 c and d. Combined with K_s and L' data (Marois et al. 2010) and our new 3.3 μm data, this indicates that HR 8799 e has similar atmospheric properties to HR 8799 c and d. The planets are all brighter than expected at 3.3 μm, where equilibrium chemistry models predict that CH$_4$ opacity should make the planets faint.

We model the HR 8799 planets with thick-cloudy atmospheres (Madhusudhan et al. 2011) and allow the CO and CH$_4$ mixing ratios to vary arbitrarily. The models that fit our 3.3 μm data (which have very little CH$_4$) substantially overpredict the planets' fluxes at L' (3.8 μm). Hotter atmospheres (>1300 K) have a similar 3.3 μm–3.8 μm color as the HR 8799 planets, and the *shape* of the Barman et al. (2011a) *HK* spectrum is also well fit by an atmosphere that is significantly hotter than indicated

by the HR 8799 planets' bolometric magnitudes. As a result, we consider the possibility that small sections of the planets' atmospheres are hot (>1300 K), dominating the shape of the SEDs, while the majority of the planets' atmospheres are cooler and do not produce much flux. The temperature–pressure profile must be the same between the "hot" and "cool" regions, so the physical difference would be that the "cool" regions have increased cloud opacity. Since the SED is consistent with a cloudy atmosphere, the "hot" regions must also be cloudy, so the combined atmosphere is composed of mixed clouds, some of which are thicker than others. Our mixed-cloud models are able to fit all of the HR 8799 data. However, we caution that our models are not fully self-consistent and that more theoretical work is necessary to validate our hypothesis.

The HR 8799 planets have unusual SEDs that are not well fit by the same models that have been used to fit field brown dwarfs. From an observational standpoint, *HK* spectroscopy and 3.3 μm−L' colors have been particularly powerful in ruling out model atmospheres. *HK* spectroscopy of HR 8799 cde, and other directly imaged planets in general, is critical to our understanding of clouds and non-equilibrium chemistry. We also note that, given the wide range of 3–4 μm SEDs predicted by the models in this paper, it would be very useful to obtain low-resolution spectroscopy of the HR 8799 planets in this range. From a theoretical standpoint, our new 3.3 μm photometry is a challenge even for non-equilibrium chemistry models, which predict bright 3.3 μm photometry. Mixed-cloud models are one possible way to flatten out 3.3 μm–3.8 μm photometry and hide CH$_4$ opacity.

REFERENCES

Baraffe, I., Chabrier, G., Barman, T. S., Allard, F., & Hauschildt, P. H. 2003, A&A, 402, 701
Barman, T. S., Macintosh, B., Konopacky, Q. M., & Marois, C. 2011a, ApJ, 733, 65

Barman, T. S., Macintosh, B., Konopacky, Q. M., & Marois, C. 2011b, ApJ, 735, L39

Bowler, B. P., Liu, M. C., Dupuy, T. J., & Cushing, M. C. 2010, ApJ, 723, 850

Burgasser, A. J., Marley, M. S., Ackerman, A. S., et al. 2002, ApJ, 571, L151

Burrows, A., Marley, M., Hubbard, W. B., et al. 1997, ApJ, 491, 856

Burrows, A., Sudarsky, D., & Hubeny, I. 2006, ApJ, 640, 1063

Burrows, A., Sudarsky, D., & Lunine, J. I. 2003, ApJ, 596, 587

Chabrier, G., Baraffe, I., Allard, F., & Hauschildt, P. 2000, ApJ, 542, 464

Chauvin, G., Lagrange, A.-M., Dumas, C., et al. 2004, A&A, 425, L29

Cohen, M., Walker, R. G., Barlow, M. J., & Deacon, J. R. 1992, AJ, 104, 1650

Cowley, A., Cowley, C., Jaschek, M., & Jaschek, C. 1969, AJ, 74, 375

Currie, T., Burrows, A., Itoh, Y., et al. 2011, ApJ, 729, 128

Dodson-Robinson, S. E., Veras, D., Ford, E. B., & Beichman, C. A. 2009, ApJ, 707, 79

Dupuy, T. J., & Liu, M. C. 2012, arXiv:1201.2465

Esposito, S., Mesa, D., Skemer, A., et al. 2012, arXiv:1203.2735

Esposito, S., Riccardi, A., Pinna, E., et al. 2011, Proc. SPIE, 8149, 814902

Esposito, S., Riccardi, A., Quirós-Pacheco, F., et al. 2010, Appl. Opt., 49, G174

Fabrycky, D. C., & Murray-Clay, R. A. 2010, ApJ, 710, 1408

Galicher, R., Marois, C., Macintosh, B., Barman, T., & Konopacky, Q. 2011, ApJ, 739, L41

Geballe, T. R., Knapp, G. R., Leggett, S. K., et al. 2002, ApJ, 564, 466

Gray, R. O., & Kaye, A. B. 1999, AJ, 118, 2993

Heinze, A. N., Hinz, P. M., Kenworthy, M., Miller, D., & Sivanandam, S. 2008, ApJ, 688, 583

Hinkley, S., Carpenter, J. M., Ireland, M. J., & Kraus, A. L. 2011, ApJ, 730, L21

Hinz, P. M., Bippert-Plymate, T., Breuninger, A., et al. 2008, Proc. SPIE, 7013, 701328

Hinz, P. M., Rodigas, T. J., Kenworthy, M. A., et al. 2010, ApJ, 716, 417

Janson, M., Bergfors, C., Goto, M., Brandner, W., & Lafrenière, D. 2010, ApJ, 710, L35

Knapp, G. R., Leggett, S. K., Fan, X., et al. 2004, AJ, 127, 3553

Kratter, K. M., Murray-Clay, R. A., & Youdin, A. N. 2010, ApJ, 710, 1375

Lafrenière, D., Marois, C., Doyon, R., Nadeau, D., & Artigau, É. 2007, ApJ, 660, 770

Leggett, S. K., Golimowski, D. A., Fan, X., et al. 2002, ApJ, 564, 452

Lloyd-Hart, M. 2000, PASP, 112, 264

Madhusudhan, N., Burrows, A., & Currie, T. 2011, ApJ, 737, 34

Malbet, F., Yu, J. W., & Shao, M. 1995, PASP, 107, 386

Marley, M. S., Saumon, D., & Goldblatt, C. 2010, ApJ, 723, L117

Marois, C., Lafrenière, D., Doyon, R., Macintosh, B., & Nadeau, D. 2006, ApJ, 641, 556

Marois, C., Macintosh, B., Barman, T., et al. 2008, Science, 322, 1348

Marois, C., Zuckerman, B., Konopacky, Q. M., Macintosh, B., & Barman, T. 2010, Nature, 468, 1080

McCarthy, D. W., Jr., Ge, J., Hinz, J. L., Finn, R. A., & de Jong, R. S. 2001, PASP, 113, 353

Metchev, S., Marois, C., & Zuckerman, B. 2009, ApJ, 705, L204

Moór, A., Ábrahám, P., Derekas, A., et al. 2006, ApJ, 644, 525

Moro-Martín, A., Rieke, G. H., & Su, K. Y. L. 2010, ApJ, 721, L199

Moya, A., Amado, P. J., Barrado, D., et al. 2010, MNRAS, 405, L81

Saumon, D., & Marley, M. S. 2008, ApJ, 689, 1327

Skemer, A. J., Close, L. M., Szűcs, L., et al. 2011, ApJ, 732, 107

Skrutskie, M. F., Jones, T., Hinz, P., et al. 2010, Proc. SPIE, 7735, 77353H

Su, K. Y. L., Rieke, G. H., Stapelfeldt, K. R., et al. 2009, ApJ, 705, 314

Sudol, J. J., & Haghighipour, N. 2012, arXiv:1201.0561

Westphal, J. A. 1969, ApJ, 157, L63

Zuckerman, B., Rhee, J. H., Song, I., & Bessell, M. S. 2011, ApJ, 732, 61